A Power-Angle-Spectrum Based Clustering and Tracking Algorithm for Time-varying Radio Channels

Chen Huang, *Student Member, IEEE,* Ruisi He, *Senior Member, IEEE,* Zhangdui Zhong, *Senior Member, IEEE,* Bo Ai, *Senior Member, IEEE,* Yangli-Ao Geng, Zhimeng Zhong, *Member, IEEE,* Qingyong Li, *Member, IEEE,* Katsuyuki Haneda, *Member, IEEE,* Claude Oestges, *Fellow, IEEE*

***Abstract*—Radio channel modeling has been an important research topic, since the performance of any communication system depends on channel characteristics. So far, most existing clustering algorithms are conducted based on the multipath components (MPCs) extracted by using a high-resolution parameter estimation approach, e.g., SAGE or MUSIC, etc. However, most of the estimation approaches require prior information to extract MPCs. Moreover, the high-resolution estimation approaches usually result in relatively high complexity and thus the clusters can only be identified by using an off-line approach after the measurements. Therefore, a power angle spectrum based clustering and tracking algorithm (PASCT) is proposed in this paper. First, a power angle spectrum (PAS) is extracted from measurement data by using a Bartlett beamformer. For each PAS, the potential targets are selected from the background and separated into clusters by using image processing approaches. The recognized clusters are characterized by three attributes: i) size, ii) position, and iii) shape feature, where orientation histogram is developed to describe the shape feature of the clusters. Moreover, a cost minimizing tracking approach based on Kuhn-Munkres method is proposed to accurately identify the clusters in non-stationary channels. The proposed PASCT algorithm is validated based on both simulations and measurements. It is found that the dominating clusters in both line-of-sight and non-line-of-sight environments can be well recognized and tracked with the proposed algorithm. By using the proposed algorithm, the dynamic changes of the clusters in real-time channel measurements, e.g., number, birth-death process, and size of the clusters, can be well observed. Through the experiments, the proposed algorithm can achieve fairly good accuracy on the cluster identification with lower complexity compared to the conventional solution.**

***Index Terms*—Channel measurement and modeling, clustering and tracking analysis, target recognition, multipath component.**

I. Introduction

CHANNEL modeling is one of the most important basic research areas in radio communications, considering the performance of any practical system depends on channel characteristics. The main goal of channel modeling is to characterize the multipath components (MPCs) in various environments. Due to the movements of communication terminals or the dynamic changes of environments, time-varying channel characterizations usually meet great challenges. However, many communication systems are operating in dynamic environments, e.g., vehicle-to-vehicle communications [1]. On the other hand, a large body of multiple-input-multiple-output (MIMO) measurements have shown that the MPCs are generally distributed in groups, also known as clustered, e.g., [2]. Hence, many recent radio channel models are based on the concept of cluster, e.g., the Saleh-Valenzuela model [3], COST 2100 [4], 3GPP Spatial Channel Model [5] and WINNER [6], etc., where the cluster has been usually considered as a group of MPCs with similar channel parameters [7]–[9]. Hence, dynamic clustering algorithms are required to develop the time-varying channel models.

To develop the cluster-based time-varying channel models, the clusters of MPCs need to be accurately identified. In the past, visual inspection has been widely used [10]. However, it has some limitations: i) the objective clustering criteria are generally missing and the results depend on the operator; ii) it is too time-consuming for the clustering process of a large number of data, especially in the time-varying channels. Therefore, automatic clustering algorithms have drawn a lot of attention. Some clustering algorithms for MPCs are developed in [11], [12], where clusters are identified based on the characterization of power delay profile (PDP). However, the directional feature of signals has not been fully used in the research, which is an important feature in MIMO radio channels. Meanwhile, clustering analysis is a hot research topic in the field of machine learning [13]–[15]. The KPowerMeans method [16] is proposed to cluster MPCs in static channels, which is based on the conventional KMeans algorithm. Similarly, an automatic MPC clustering algorithm is proposed in [17] based on kernel power density estimation of MPCs, where the directional characteristic is used to recognize clusters. As for the clustering algorithm for the time-varying channels, the MPCs not only need to be clustered but also need to be tracked, where minimum distance based tracking and clustering approach has been widely used

C. Huang, Y.-A. Geng and Q. Li are with the School of Computer and Information Technology, Beijing Jiaotong University, Beijing 100044, China (e-mail: morning@bjtu.edu.cn; gengyla@bjtu.edu.cn; liqy@bjtu.edu.cn).

R. He, Z. Zhong, B. Ai are with the State Key Laboratory of Rail Traffic Control and Safety, Beijing Jiaotong University, Beijing 100044, China (e-mail: ruisi.he@bjtu.edu.cn; zhdzhong@bjtu.edu.cn).

Z. Zhong is with the Huawei Technologies Ltd., Shanghai 210206, China (e-mail: zhongzhimeng@huawei.com).

K. Haneda is with the Department of Radio Science and Engineering, Aalto University, 00076 Aalto, Finland (e-mail: katsuyuki.haneda@aalto.fi).

C. Oestges is with the Institute of Information and Communication Technologies, Electronics and Applied Mathematics, Universite Catholique de Louvain, 1348 Louvain-la-Neuve, Belgium (e-mail:claude.oestges@uclouvain.be).

in the past, e.g., [18]–[20]. Most of these studies identified the clusters based on the obtained MPCs, where MPCs need to be extracted in advance by using a high-resolution multi-path parameters estimation algorithm, e.g., space-alternating generalized expectation-maximization (SAGE) [21], CLEAN [22], joint maximum likelihood estimation (RiMAX) [23] or iterative nonlinear least square approximation (INLSA) [24], [25].

Nevertheless, performing the high-resolution estimation usually is time-consuming, which is thus used as for the off-line processing of measurements. Besides, most of the high-resolution estimation algorithms are sensitive to the prior parameters, where a small change of the prior parameters may lead to different results. For example, to efficiently extract MPCs, the number of MPCs is usually required for the SAGE algorithm as an initial parameter for each snapshot, which is mostly unavailable. It is generally difficult to have the specific prior information for MPC extractions, especially considering a large number of snapshots measured in time-varying channels. Meanwhile, estimation algorithms such as the Bartlett beamformer [26] can be conducted much faster and provides spectral estimation results, which can be conducted with lower computational complexity and provide referential information for parameters extraction or channel modeling, e.g., geometric position and power distribution of MPCs, etc. So far, there still lacks accurate clustering algorithms based on spectral estimation results. Hence, a low cost algorithm for a joint beamformer and clustering in time-varying channels is required.

On the other hand, target recognition and clustering analysis are hot research topics in the field of machine learning [13], considerable effort has to be made to adapt the results to clustering of MPCs in wireless channels. In our previous work of [27], we briefly introduce the idea of recognizing the clusters in a power angle spectrum (PAS) without using any high-resolution estimation algorithm. In this paper, we extend our previous work and propose a novel cluster recognition and tracking algorithm, which selects target objects based on the power distribution of the elements in PAS, and further separates clusters in each target object based on the power distribution in each target object. Note that, the target object here denotes the gathered elements having higher power than background noise, which may contain one or more clusters. To accurately track the clusters in the time-varying channels, we characterize the clusters with three attributes: i) size of the cluster in angle domain, which reflects the angular spread of the clusters; ii) mass center of the cluster, which is power weighted cluster centroid; iii) shape feature of the recognized cluster. Specifically, orientation histogram (OH) [30] is innovatively developed to characterize the shape and power distribution features of the clusters. By using the three attributes, a cost function is defined for tracking clusters over time, where the moving paths of clusters can be accurately found.

The rest of this paper is organized as follows. In Section II, the measurement campaign in suburban crossroad scenarios and problem description are presented. Sections III and IV present the proposed cluster recognition and tracking algorithms, respectively. Section V gives the results of the proposed algorithm based on both the simulation data and the measurement data. Besides, the computational complexity of the proposed algorithm is also validated in Section V. Finally, conclusions are drawn in Section VI.

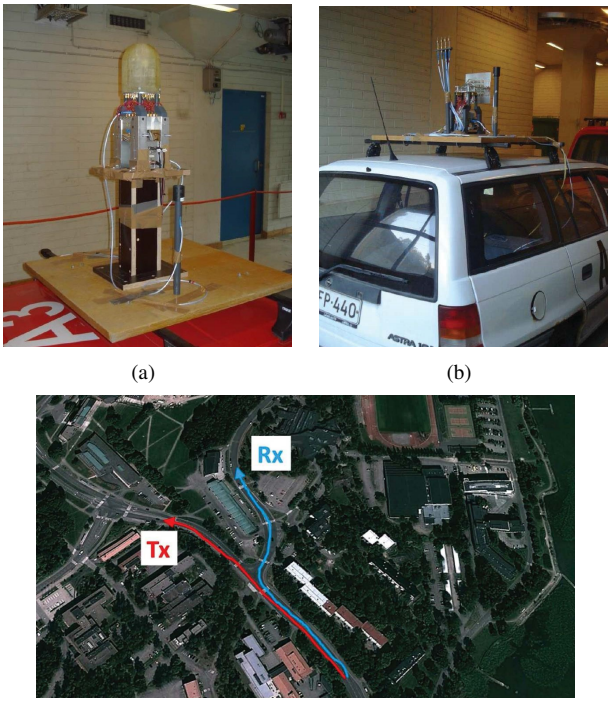

(a) (b)

(c)

Fig. 1. Antenna arrays. (a) Semispherical antenna array at the Rx side. (b) ULA at the Tx side (c) Maps of the measurements in the cross-road scenarios [35].

II. Problem Description

In this section, we first briefly introduce the environment and system parameters of the measurement campaign. Then, the motivation and the framework of this study is presented.

A. Data Collection

The measurements were conducted with Aalto channel sounder [33] at 5.3 GHz using a bandwidth of 60 MHz. The main system parameters are summarized in Table I. The antenna arrays are shown in Figs. 1(a)-(b). A dual-polarized semispherical antenna array was used at the receive (Rx) side, which consists of 15 dual-polarized elements. A uniform linear array (ULA) with four vertically polarized antennas was used at the transmit (Tx) side. Therefore, the measured MIMO channel matrix was $N_{Rx} \times N_{Tx} = 30 \times 4$. The uniform spacing of the antenna array is $\lambda/2$, where the width of the main lobe of the beamformer is $2\pi/15$. More details of the channel sounder and measurements can be found in [33]–[35]. The Tx and Rx antenna arrays were mounted on top of a wooden platform on the roof of two compact cars, and the antenna height was approximately 2.20 m above ground.

The measurement campaign was conducted in the suburban area of Tapiola, Finland, whose top view is shown in Fig.

TABLE I
SYSTEM PARAMETERS

Parameter	Value
Center frequency	5.3 GHz
Transmit power	36 dBm
Measurement bandwidth	60 MHz
Sampling frequency	120 MHz
Delay resolution	16.7 ns
Snapshot interval	15 ms

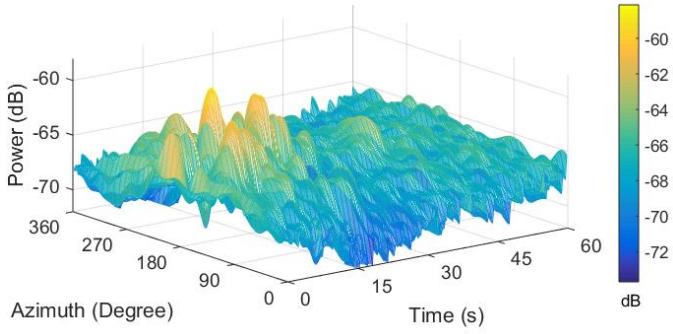

(a)

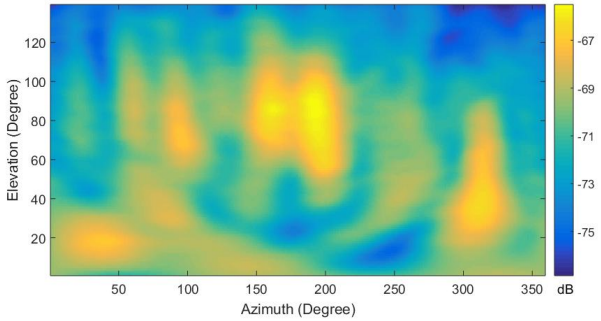

(b)

Fig. 2. PASs (in dB) extracted from measurement data. (a) shows the extracted PASs during continuous time for cross-road scenario and (b) is a sample of PAS collected at 37.5 s.

1(c). During the experiment, the vehicles average speed was 10 km/h, and the traffic was between light and medium. The duration for a measurement route was generally between 55 s and 65 s, which approximately corresponds to a maximum traveled distance on the order of 210 m - 250 m. In the measurements, two cars were traveling in separate directions after passing the cross-road, as in Fig. 1(c). Before they separate, the Rx car was always traveling ahead of the Tx one. In this case, after the two cars separate, the Tx and Rx vehicles are surrounded by distinct scattering environments that keep varying over time independently, and the line-of-sight (LoS) is fully blocked by roadside buildings and trees.

B. Problem Description

The PAS can be obtained by using the Bartlett beamformer [26], as expressed as

$$PAS(t) = \frac{[c(\Omega,t)]^H \mathbf{R} [c(\Omega,t)]}{[c(\Omega,t)]^H [c(\Omega,t)]} \quad (1)$$

where $c(\Omega,t)$ is the steering vector for the Rx at time t, $\Omega = [\cos(\phi_1)\sin(\phi_2), \sin(\phi_1)\sin(\phi_2), \cos(\phi_2)]$, ϕ_1, ϕ_2 are azimuth of arrival and elevation of arrival, respectively, and $\mathbf{R}$ is the spatial covariance matrix, defined as

$$\mathbf{R} = \mathrm{E}\{\mathbf{H}_{\mathrm{meas}} \mathbf{H}_{\mathrm{meas}}^{\mathrm{H}}\} \quad (2)$$

where $\mathrm{E}\{\cdot\}$ is the expectation operation for all channel realizations. It is noteworthy that we averaged $\mathbf{R}$ over the four Tx antennas, and there are 513 frequency samples averaged over to estimate $\mathbf{R}$.

In this case, the PAS for each snapshot consists of elements $\alpha(\phi_1, \phi_2, t)$, $\phi_1 \in (0°, 360°]$, $\phi_2 \in (0°, 180°]$, and the total number of angle grid points are 16200 in each snapshot, where a spacing of 2 degrees is used both in azimuth and elevation. The PASs of the whole consecutive snapshots are shown in Fig. 2(a), whereas Fig. 2(b) is a sample of PASs at one time instant during the movement of the Rx on the car. Note that, to easily observe the dynamic changes of directional features during snapshots, the power in azimuth domain of different snapshots are plotted in Fig. 2(a), whereas the amplitudes in elevation domain are summed in each azimuth degree. As mentioned before, the cluster is generally defined as a group of MPCs having similar parameters, which is similar to the definition in [16], [17] and has been widely used as in [18], [19]. The study in [36] shows that the identification of the cluster in the double directional/angle domain has a higher resolution than the angle-delay domain. Therefore, to ensure the trade-off between computational complexity and accuracy, the PAS is obtained in the azimuth-elevation domains by averaging the power in the delay domain. From Fig. 2(a), it is found that the measurement data before 34.5s is collected in LoS scenario (before the cars separated) where most signals are strong and clear; whereas the measurement data after 34.5s is collected in NLoS scenario (after the car separated).

The main goal of the proposed PASCT algorithm is to first recognize and identify clusters in each PAS, e.g., Fig. 2(b), and secondly track the identified clusters during consecutive snapshots. To achieve this goal, this paper presents a two-stage target recognition based automatic clustering and tracking algorithm: in the first stage, a heuristic approach is used to select target objects, which may contain one or more clusters, based on the power distribution of the elements in the PAS. Then a cluster separation approach is applied to further accurately separate clusters by considering the power distribution in each selected target object. In the second stage, we use inherent attributes of clusters to describe the separated clusters, where OH are innovatively developed to characterize the shape and the power distribution feature of the clusters in PASs. Moreover, instead of using the minimized distance based tracking approach [18]–[20], a global minimizing cost based tracking approach is proposed to track the clusters in the time-varying channels as described in Section IV.

III. CLUSTER RECOGNITION

In this section, a target recognition based clustering approach is proposed, which is found to be able to well recognize the clusters in both LoS and NLoS scenarios. Generally,

to recognize the clusters from PAS, we need to distinguish between clusters and background. In this case, the power distribution feature of the cluster can be used to distinguish the clusters from the background. Here, the maximum-between-class-variance method is used to recognize clusters in PAS. Nevertheless, the clusters close to each other tend to be recognized as one big target, which is called as a target object. In this case, to further recognize clusters in the big target objects, a density-peak-searching method is developed to divide the clusters. The details of the clustering process are clearly expressed as follows.

A. Target Recognition

To avoid the computation cost caused by using a high-resolution estimation algorithm, the proposed PASCT algorithm is designed to recognize clusters based on the PAS obtained by using low-resolution estimation algorithm. To recognize the target objects in PAS, the maximum-between-class-variance method [28] is applied to automatically determine a selection threshold of power for the elements in the PAS, which can separate the target objects from the background noise at the first stage. Let $[\alpha'_1, \alpha'_2, \cdots, \alpha'_L]$ denote different power levels in one PAS, which are evenly distributed in $[\min\{\alpha(\phi_1, \phi_2, t)\}, \max\{\alpha(\phi_1, \phi_2, t)\}]$. There are $n_{\alpha'_i}$ elements having the power of level α'_i, $i \in [1, L]$, thus the total number of elements is $N_\alpha = n_{\alpha'_1} + n_{\alpha'_2} + \cdots + n_{\alpha'_L}$. The probability distribution of the *normalized* power in one PAS can be expressed as

$$p_{\alpha'_i} = n_{\alpha'_i}/N_\alpha, \quad p_{\alpha'_i} \geq 0, \sum_{\alpha'_i=\alpha'_1}^{\alpha'_L} p_{\alpha'_i} = 1. \tag{3}$$

To separate the target objects from the background, let α'_T denotes the separation threshold, where the power levels of background noise and target objects are $[\alpha'_1, \alpha'_2, \cdots, \alpha'_T]$ and $[\alpha'_{T+1}, \cdots, \alpha'_L]$, respectively. Therefore, the probabilities of the background noise and target objects occurrence in the current PAS can be expressed by p_B and p_O, as follows

$$p_B(\alpha'_T) = \sum_{\alpha'_i=\alpha'_1}^{\alpha'_T} p_{\alpha'_i} \tag{4}$$

$$p_O(\alpha'_T) = \sum_{\alpha'_i=\alpha'_{T+1}}^{\alpha'_L} p_{\alpha'_i} \tag{5}$$

and the average power levels of background noise and target objects are given by

$$e_B(\alpha'_T) = \sum_{\alpha'_i=1}^{\alpha'_T} \alpha'_i p_{\alpha'_i}/p_B(\alpha'_T) \tag{6}$$

$$e_O(\alpha'_T) = \sum_{\alpha'_i=\alpha'_{T+1}}^{\alpha'_L} \alpha'_i p_{\alpha'_i}/p_O(\alpha'_T). \tag{7}$$

It can be easily verified that the following relation holds for the separation threshold α'_T:

$$p_B(\alpha'_T)e_B(\alpha'_T) + p_O(\alpha'_T)e_O(\alpha'_T) = E(\alpha'_i) \tag{8}$$

$$p_B(\alpha'_T) + p_O(\alpha'_T) = 1 \tag{9}$$

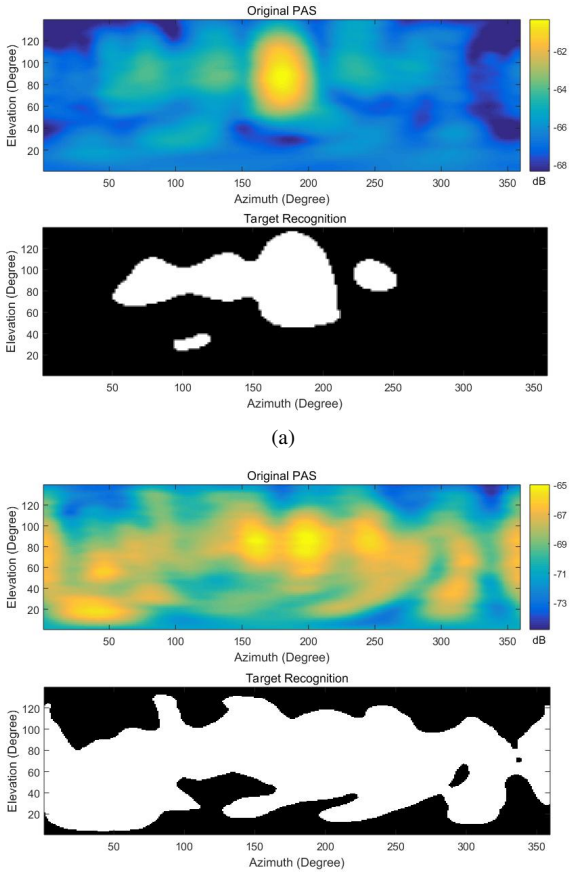

Fig. 3. Original PASs based on measurement data and target recognition results for different scenarios, where (a) and (b) are samples of PAS (in dB) in LoS scenario and NLoS scenario, respectively.

where $E(\alpha'_i)$ is the total mean power level of all the elements in the PAS, which is equal to $\sum_{\alpha'_i=\alpha'_1}^{\alpha'_L} \alpha'_i p_{\alpha'_i}$. The between-class-variance [28] of the average power levels of background noise and target objects can be expressed by

$$\begin{aligned}\delta^2(\alpha'_T) = {} & p_B(\alpha'_T)(e_B(\alpha'_T) - E(\alpha'_i))^2 \\ & + p_O(\alpha'_T)(e_O(\alpha'_T) - E(\alpha'_i))^2.\end{aligned} \tag{10}$$

From (8), (9) and (10), $\delta^2(\alpha'_T)$ can be rewritten as

$$\delta^2(\alpha'_T) = p_B(\alpha'_T)p_O(\alpha'_T)(e_B(\alpha'_T) - e_O(\alpha'_T))^2. \tag{11}$$

The difference between background noise and groups of clusters can be maximized by maximizing the between-class-variance, and the best selection threshold ${\alpha'_T}^*$ can be therefore expressed as

$${\alpha'_T}^* = \arg\{\max \delta^2(\alpha'_T) | \alpha'_1 \leq \alpha'_T < \alpha'_L\}. \tag{12}$$

Since the number of the power levels is limited, thus ${\alpha'_T}^*$ can be easily found by the sequential search, and thus the target objects which may consist of clusters can be separated from the background noise by using a selection threshold ${\alpha'_T}^*$.

Nevertheless, the signal to interference plus noise ratio (SINR) of PAS has a strong impact on the performance of the target recognition. Fig. 3 shows two examples of conducting the targets recognition approach based on the measurement

data introduced in Section II, where the black and white areas in target recognition results represent the background and detected targets, respectively. In the LoS scenario, as shown in Fig. 3(a), as the clusters are generally clear with strong power and low background noise, the targets can be easily recognized and detected. However, in the NLoS scenario, the power distribution of the PAS is more complicated with high background noise, and many small clusters caused by reflections and scatterings interfere the recognition process, e.g., as shown in the original PAS of Fig. 3(b). In this case, these small clusters are easy to be recognized as one big target, i.e., the target recognition result in Fig. 3(b), which brings significant difficulties to distinguish clusters from the targets. To avoid recognizing NLoS clusters as one big target object, an observation window $\Delta\alpha'_W$ is set so that only the elements having the power level between $[\alpha'_L - \Delta\alpha'_W, \cdots, \alpha'_L]$ are processed in the targets recognition approach. In this case, the best selection threshold ${\alpha'_T}^*$ is obtained by

$${\alpha'_T}^* = \arg\{\max \delta^2(\alpha'_T) | \alpha'_L - \Delta\alpha'_W \leq \alpha'_T < \alpha'_L\}. \quad (13)$$

By using the observation window, the recognition process can focus on the elements with stronger power over the noise background. Moreover, a heuristic sequential search is used to select an appropriate observation window size $\Delta\alpha'_W$ as follows. Parameter $\Delta\alpha'_W$ is initialized to $0.1\alpha'_L$ at the beginning of the searching process and keeps increasing until the following constraints are no longer satisfied:

- Size of recognized targets: $S^{\mathrm{T}}_{\min} < S_{\min}, S_{\max} < S^{\mathrm{T}}_{\max}$
- Power gap of each single target: $\Delta A < \Delta A_{\max}$

where $S_{\min}$ and $S_{\max}$ are the smallest and biggest size of the recognized targets indicating how many elements the target consists of, and $S^{\mathrm{T}}_{\min}$, $S^{\mathrm{T}}_{\max}$ is the lower and upper limit of size. Such that, to avoid the interference caused by the small and fragmental targets, which are more like noises than clusters, the lower limit of the size is also considered, only the target bigger than $S^{\mathrm{T}}_{\min}$ is counted. Parameter ΔA is the gap between the highest power and the mean power of each target. In each iteration, S and ΔA are updated based on the recognized target objects by using the new ${\alpha'_T}^*$ from (13), until the above constraints are no longer satisfied.

From our experiments based on the measured data, $S^{\mathrm{T}}_{\max}$ and $\Delta A_{\max}$ are found to be generally increased with the increase of $\Delta\alpha'_W$, where an oversize observation window also tends to cause recognizing many small targets as one big object. Based on the preset of $S^{\mathrm{T}}_{\min}$, $S^{\mathrm{T}}_{\max}$ and $\Delta A_{\max}$, proper targets can be well recognized, i.e., Fig. 4(a). Comparing with a whole PAS, the obtained targets are easier to further separate into more accurate clusters. Note that, based on the experiments, the step size of the increased $\Delta\alpha'_W$ is suggested to be $0.1\alpha'_L$.

B. Cluster Separation

As shown in Fig. 4(a), the targets can be well recognized. However, each target may still contain one or more clusters. Therefore, to further separate the recognized targets into more accurate clusters, we propose the density-peak-searching method based on the clustering method in [29].

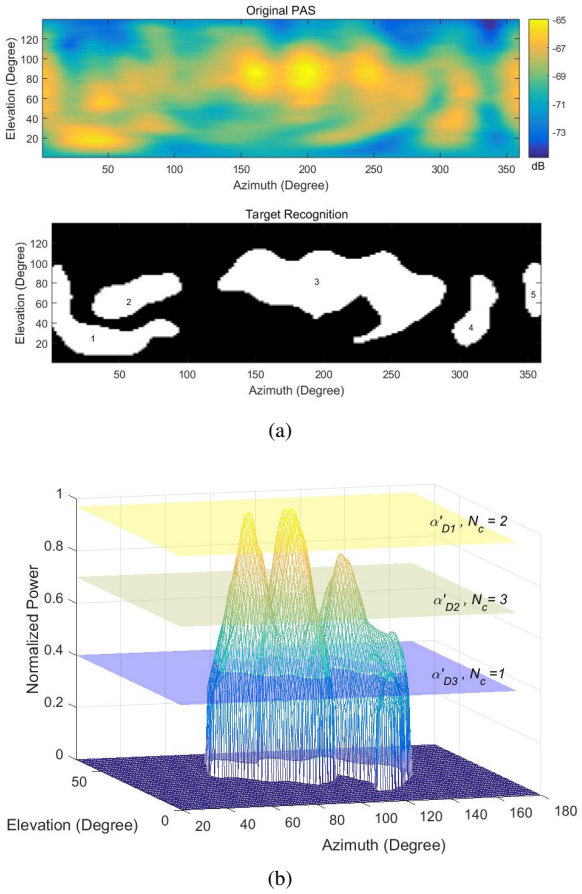

Fig. 4. (a) shows target recognition result for the PAS (in dB) based on NLoS measurement data, where $\Delta\alpha'_W$ is selected by using the proposed heuristic approach. (b) shows mesh diagram of the recognized target 3 in (a), where three detecting planes with different values of D_i are applied to detect the number of clusters N_c.

First, the number of clusters in each processed target needs to be predetermined, which is obtained by setting a threshold α'_D. Fig. 4(b) shows the mesh diagram of the recognized target 3 in Fig. 4(a), and three detecting planes with different values of α'_D are used to cut the mesh diagram. In this case, the clusters can be found by observing the cross sections and the elements with the power higher than α'_D. With the decreasing of α'_D from the maximum power in the target, and the number of the obtained clusters generally increases first and decreases later due to the power distribution feature of the targets. In this case, α'_D is selected so that the most clusters can be obtained, as follows

$${\alpha'_D}^* = \arg\max_{\alpha'_D} N_c \quad (14)$$

where N_c is the number of the obtained clusters. In this case, α'_{D2} is the best threshold in Fig. 4(b), where the most clusters are obtained. Note that, the step size of changing threshold α'_D is set to $0.1\alpha^a_{\max}$, where $\alpha^a_{\max}$ is the maximum power in the ath cluster.

Such that, the main clusters in each target object are first obtained by applying the threshold ${\alpha'_D}^*$, where the elements in each main cluster are also clustered at the meantime. The remaining elements in each target object but not belonging

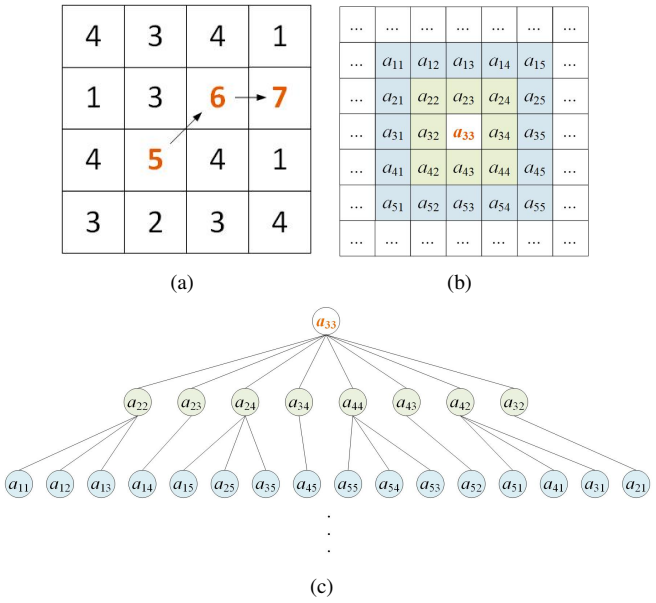

Fig. 5. Illustration of the clustering strategy. In (a), element 5 is clustered with element 6 which is the adjoining neighbor with highest power, whereas elements 5, 6 are then clustered with element 7 similarly. (b) is an example of BFS searching sequence starting from a_{33}, where (c) gives the search tree.

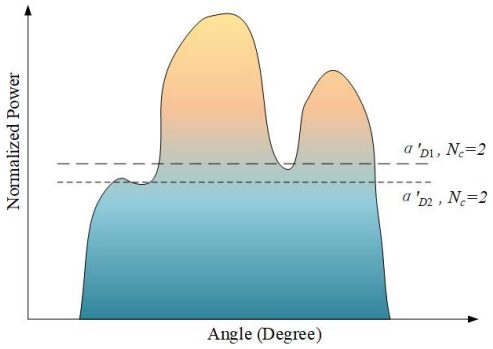

Fig. 6. An example of obtaining the number of clusters, where different results but with the same cluster number can be obtained by using α'_{D1} and α'_{D2}, respectively.

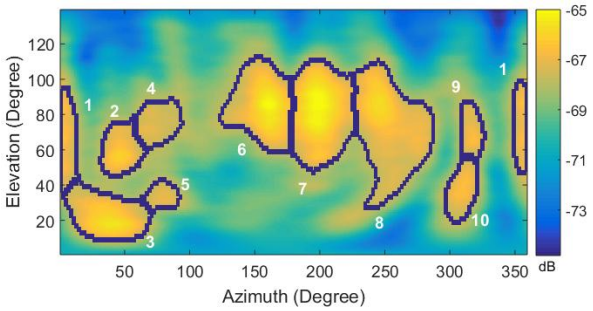

Fig. 7. The cluster recognition result for the PAS (in dB) sample used in Fig. 4(a).

to any main cluster need to be clustered. The key idea is to cluster each element with its adjoining element, which has the strongest power. Moreover, breadth-first search (BFS) [37] is used to search the closest neighboring element with the strongest power. Figs. 5(a)-(c) illustrate the attaching process of the density-peak-search, where the number represents the power level, and the clustering relationship is represented by arrows. As shown in Fig. 5(a), element 5 is clustered with its adjoining element 6, which has the highest power among the eight adjoining neighbors. And similarly, elements 5 and 6 are then clustered to element 7. Such that each element is eventually clustered within a cluster obtained by ${\alpha'_D}^*$. Fig. 5(b) shows an example of BFS searching sequence starting from a_{33}, where Fig. 5(c) presents the search tree for the case in Fig. 5(b). It is noteworthy that multiple α'_D may obtain different clusters with the same number of clusters in some cases, as shown in Fig. 6. Both α'_{D1} and α'_{D2} can obtain two clusters, but the clustering results are different by using BFS. Considering that the cluster with higher power generally has more influences to the channel, the threshold which can obtain the clusters with higher average power is thus selected, which is α'_{D1} in Fig. 6.

Due to the periodicity of the azimuth, the cluster around 0 degree may be split into two clusters in the PAS, e.g., the targets 1 and 5 in Fig. 4(a). In this case, a merging process is introduced to merge these clusters. The main idea of the merging process is to measure the clusters if they coincide on the 0 degree boundary. If two clusters a and b coincide with each other on the 0 degree boundary, which contains N'_a and N'_b elements on the boundary, respectively, and the number of adjoint elements pairs (overlapping length) is $N'_{a\bigcap b}$. Then, these clusters are merged into one if

$$N'_{a\bigcap b} > 90\% \min\{N'_a, N'_b\}. \tag{15}$$

By using the density-peak-search approach, the recognized target is further separated into more accurate clusters, e.g., the cluster recognition results in Fig. 7, where cluster 1 is identified across the boundary, and further validation of clustering performance is presented in Section V.

IV. Cluster Tracking

In this section, we propose a minimizing cost based cluster tracking approach, which is found to be able to track the clusters in the time-varying channels. To track the clusters in consecutive snapshots, the feature of clusters needs to be extracted to determine whether the clusters appear, disappear or move. Such that, each cluster is characterized by three features: size, position (in azimuth and elevation domains) and shape. Based on the three features, the moving cost is proposed to search the most likely moving path of each cluster. The detail of the tracking process is expressed as follows.

A. Cluster Feature

To accurately track the clusters in the time-varying channels, the clusters need to be properly characterized first. When using visual inspection, the position and shape of the clusters are the key features to track the clusters in consecutive PASs. Inspired by visual inspection and considering the cluster recognition process, three characteristics are proposed to describe the recognized clusters, as follows:

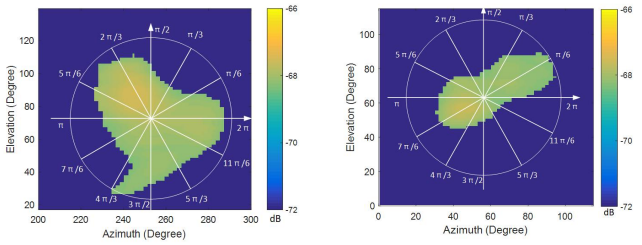

(a) (b)

Fig. 8. Illustration of OH characterization for the clusters in PAS (in dB), where (a) and (b) are two samples of the clusters in Fig. 7.

- Size of the ath recognized cluster: C_a^{N}
- Mass center of the ath recognized cluster: $\mathbf{C}_a^{\mathrm{A}}$
- Shape feature of the ath recognized cluster: $\mathbf{C}_a^{\mathrm{OH}}$

1) ***Size of the cluster:*** The total number of elements in the ath cluster is used to describe the size of this cluster, which is denoted by C_a^{N}. Generally, the size for an existing cluster does not change severely even in time-varying channels. Hence, it is an important characteristic for the clusters in the tracking process.

2) ***Mass center of the cluster:*** Instead of using geometric center, the mass center, which is the power weighted geometric center of the cluster, is used to describe the position of the cluster in the PAS, which can be obtained as follows:

$$\mathbf{C}_a^{\mathrm{A}} = \frac{\sum_{x=1}^{N_a} \alpha_x(\phi_1,\phi_2)\exp(j*\phi_{i,x})}{\sum_{x=1}^{N_a} \alpha_x(\phi_1,\phi_2)} \tag{16}$$

where $\alpha_x(\phi_1,\phi_2)$ and $\phi_{i,x}, i = 1,2$ are the power and azimuth/elevation of the xth element in the ath cluster, respectively, and N_a is the set of all elements in the ath cluster. It is noteworthy that we use a pair of complex numbers to represent the azimuth/elevation of the mass center due to the periodicity of the angle [38]. By using the mass center to describe the clusters, the tracking process can focus on the elements with high power, and the interference caused by background noise is restrained.

3) ***Shape feature of the cluster:*** When using visual inspection, the shape feature of the recognized cluster is also a prominent characteristic which contributes to identifying the clusters in consecutive snapshots. On the other hand, the histogram of oriented gradients has been widely used for human detection [30]. Inspired by the work, we develop OH feature to characterize the shape feature of the clusters in PAS. As shown in Fig. 8, each recognized cluster is observed in an individual polar coordinate system, where the cluster is divided into twelve portions with an interval of thirty degrees for each portion, and the power of elements are summed for each portion to compose a vector. In this case, the direction feature of each cluster can be expressed by the obtained vector. In this case, the shape feature of each cluster is captured and normalized into a 1×12 vector, which is comparable in the tracking process and expressed as follows:

$$\mathbf{C}_a^{\mathrm{OH}} = [\sum_{\theta=0}^{\pi/6}\alpha_{a,\theta}, \sum_{\theta=\pi/6}^{\pi/3}\alpha_{a,\theta}, \cdots, \sum_{\theta=11\pi/6}^{2\pi}\alpha_{a,\theta}] \tag{17}$$

where $\alpha_{a,\theta}$ is the power of the element in the ath cluster with the angle of θ in the polar coordinates. Note that the polar coordinates are independently set for each cluster. The mass center of the cluster is selected to be the origin of the polar coordinates, thus the OH characteristic focuses on the portions with strong power in each cluster, whereas the adverse effect caused by dynamic changing edges of the clusters can be reduced. It is noteworthy that the interval of angle can be set smaller, e.g., fifteen degrees, the cluster is therefore divided into more small portions and the dimension of $\mathbf{C}_a^{\mathrm{OH}}$ increases with the smaller interval, which results in higher accuracy of the OH characteristic, but also with higher computational complexity.

B. Cluster Tracking Approach

Based on the three characteristics, we use a generalized weighted Euclidean distance to measure the cost of the moving path between different clusters in the current and previous snapshots, which can be expressed as follows:

$$C_{a,b} = (\frac{(C_1)^r + (C_2)^r + (C_3)^r}{3})^{\frac{1}{r}} \tag{18}$$

where

$$\begin{aligned} C_1 &= \rho_1 \mathcal{N}(\Delta C_{a,b}^{\mathrm{N}}), \\ C_2 &= \rho_2 \mathcal{N}(\Delta \mathbf{C}_{a,b}^{\mathrm{A}}), \\ C_3 &= \rho_3 \mathcal{N}(\Delta \mathbf{C}_{a,b}^{\mathrm{OH}}). \end{aligned}$$

Parameters $\Delta C_{a,b}^{\mathrm{N}}, \Delta \mathbf{C}_{a,b}^{\mathrm{A}}$ and $\Delta \mathbf{C}_{a,b}^{\mathrm{OH}}$ are the Euclidean distance between the three characteristics of the ath cluster and the bth cluster, and ρ_1, ρ_2 and ρ_3 are the weight coefficients of the three characteristics. Considering that the spectrum estimation cannot promise a high resolution result and the size, and shape of the clusters in non-stationary channels may change faster than the position of the mass center of the clusters (in the angle domain), the coefficient of the mass center of the cluster is set higher than the coefficients of the size and shape, as shown in Table III. $\mathcal{N}(\cdot)$ is the normalized function which is used to compare different characteristics in the same scale, as follows:

$$\mathcal{N}(x) = \frac{x - x_{\min}}{x_{\max} - x_{\min}}. \tag{19}$$

Generally, a small $C_{a,b}$ indicates that the ath cluster is similar to the bth cluster, whereas a large $C_{a,b}$ indicates that there is much difference between the ath and bth clusters. According to *the inequality of arithmetic and geometric means* [39], $C_{a,b}$ in (18) is a monotonically increasing function with coefficient r, where upper and lower bounds are $\max(C_1, C_2, C_3)$ and $\min(C_1, C_2, C_3)$, respectively. In this case, the characteristic with more difference plays a greater influence on $C_{a,b}$. Hence, by using $C_{a,b}$ in (18), two clusters with similar size and shape feature but with obviously different position maybe considered as the same cluster by using the weighted means of (C_1, C_2, C_3), whereas they can be precisely distinguished in the proposed tracking approach.

Let $a_1, \cdots, a_{M_i}$ and $b_1, \cdots, b_{M_{i+1}}$ denote the clusters in snapshots S_i and S_{i+1}, respectively. $v(a_x, b_y)$ represents a

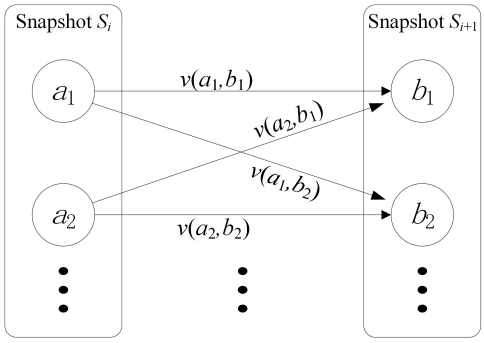

Fig. 9. Illustration of the weighted moving paths between snapshots S_i and S_{i+1}.

moving path between a_x and b_y, where $a_x \in [a_1, \cdots, a_{M_i}]$ and $b_y \in [b_1, \cdots, b_{M_{i+1}}]$. $\mathbf{V}$ represents the set of all moving paths, which can be expressed as follows:

$$\mathbf{V} = \{v(a_x, b_y) | a_x \in S_i, b_y \in S_{i+1}\}. \tag{20}$$

If there are more than one cluster during consecutive snapshots, there could be many possible moving paths between the two snapshots, whereas the most likely moving paths $\mathbf{v}^*$ is only one specific subset of the moving paths in $\mathbf{V}$. To accurately track the clusters, the cost $C_{a,b}$ is used to weight the moving path $v(a, b)$, as shown in the Fig. 9. Hence, the true moving paths $\mathbf{v}^*$ can be obtained by minimizing the total cost of all selected moving paths, as follows:

$$\mathbf{v}^* = \arg\min_{\mathbf{v} \subset \mathbf{V}} \sum_{a,b \in \mathbf{v}} C_{a,b} \tag{21}$$

where $\mathbf{v} = \{v(a_i, b_{y_i})\}_{i=1}^{M_i}$ and $y_1, y_2, \cdots, y_{M_i}$ can be any M_i permutation of integers $1, 2, \cdots, M_{i+1}$ (we assume $M_i \leq M_{i+1}$ without loss of generality). However, the number of possible choices of moving path is $M_{i+1}(M_{i+1}-1)\cdots(M_{i+1}-M_i+1)$, which can be numerous even when M_i and M_{i+1} are small.

To solve this problem, the Kuhn-Munkres (K-M) approach [31] is adopted, which is able to find the minimized weight perfect matching in a bipartite graph of a general assignment problem. In the bipartite graph, all nodes are divided into two subsets and links to each other with different weight. In this case, the recognized clusters in two consecutive snapshots and the cost of moving path are regarded as the nodes in two subsets and the linking weight, respectively. Fig. 10 is an illustration of the progress of the K-M approach for a 4×4 bipartite graph, where the cost weight of each moving path can be expressed as:

$$\mathbf{C} = \begin{bmatrix} C_{a_1,b_1} & \cdots & C_{a_1,b_4} \\ \vdots & \ddots & \vdots \\ C_{a_4,b_1} & \cdots & C_{a_4,b_4} \end{bmatrix} = \begin{bmatrix} 3 & 6 & 5 & 4 \\ 6 & 3 & 2 & 4 \\ 4 & 7 & 1 & 5 \\ 2 & 3 & 6 & 5 \end{bmatrix} \tag{22}$$

As shown in Fig. 10(a), there are two subsets $\mathbf{A}$ and $\mathbf{B}$ in the original bipartite graph and each subset contains four nodes linked to each other. The approach is initialized with the moving paths which have the minimum cost weight for each node in $\mathbf{A}$, and the value of the cost weight is stored as

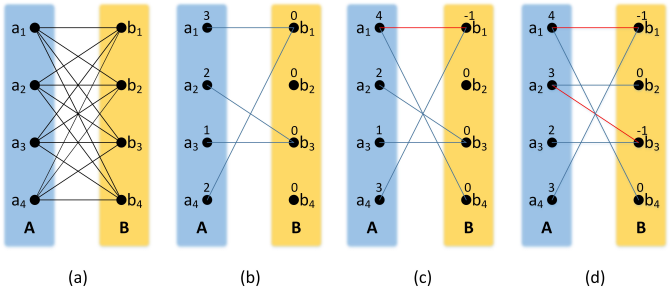

Fig. 10. Illustration of the progress of minimized cost weight perfect matching by using the K-M approach, where (a) is the original bipartite graph and (b)-(d) is three stages in matching process.

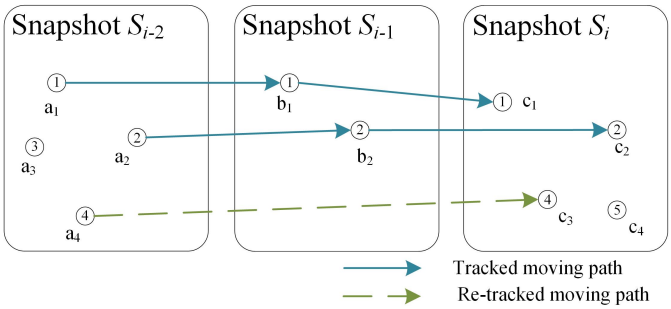

Fig. 11. Illustration of the re-track progress, where the circles and the number in them represent clusters and the tracking ID of the clusters, respectively.

the node-value v_{a_i} for the each node in $\mathbf{A}$, whereas all the node-values v_{b_i} of subset $\mathbf{B}$ are initialized to 0, as shown in Fig. 10(b). Due to the unbalanced weight cost between each node, it can always find *illegal link pair* that two nodes in $\mathbf{A}$ are linked to the same node in $\mathbf{B}$, e.g., $\{v(a_1, b_1), v(a_4, b_1)\}$ and $\{v(a_2, b_3), v(a_3, b_3)\}$ in Fig. 10(b). Let $\mathbf{U}_1$ and $\mathbf{U}_2$ represent two subsets of the nodes in $\mathbf{A}$ and $\mathbf{B}$, respectively, which appear in the illegal link pair. For the illegal pair $\{v(a_1, b_1), v(a_4, b_1)\}$, $\mathbf{U}_1 = \{a_1, a_4\}$ and $\mathbf{U}_2 = \{b_1\}$. If an illegal link pair appeared, then a new moving path is required to replace one of the moving path in the illegal link pair, which needs to satisfy the restrain in (23), as follows:

$$v(a_i, b_j) = \arg\min_{v(a_i,b_j)}(d), \quad a_i \in \mathbf{U}_1, b_j \in \mathbf{B} - \mathbf{U}_2 \tag{23}$$

where $d = C_{a_i,b_j} - v_{a_i} - v_{b_j}$, and the node-values also change with the new moving path as follows:

$$v_{a_i} = v_{a_i} + d, \ a_i \in \mathbf{U}_1 \tag{24}$$

$$v_{b_k} = v_{b_k} - d, \ b_k \in \mathbf{U}_2. \tag{25}$$

In Fig. 10(c), the moving path $v(a_1, b_4)$ achieves minimum d, thus $v(a_1, b_4)$ is adopted to replace $v(a_1, b_1)$, where v_{a_1}, v_{a_4} and v_{b_1} are also changed within the replacing process. Hence, the selected moving paths are $\mathbf{v} = \{v(a_1, b_4), v(a_2, b_3), v(a_3, b_3), v(a_4, b_1)\}$ in this stage. Obviously, $\{v(a_2, b_3), v(a_3, b_3)\}$ is another illegal pair, which can be replaced to $\{v(a_2, b_2), v(a_3, b_3)\}$ by using the same process. The final selected moving paths are $\mathbf{v}^* = \{v(a_1, b_4), v(a_2, b_2), v(a_3, b_3), v(a_4, b_1)\}$ as shown in Fig.

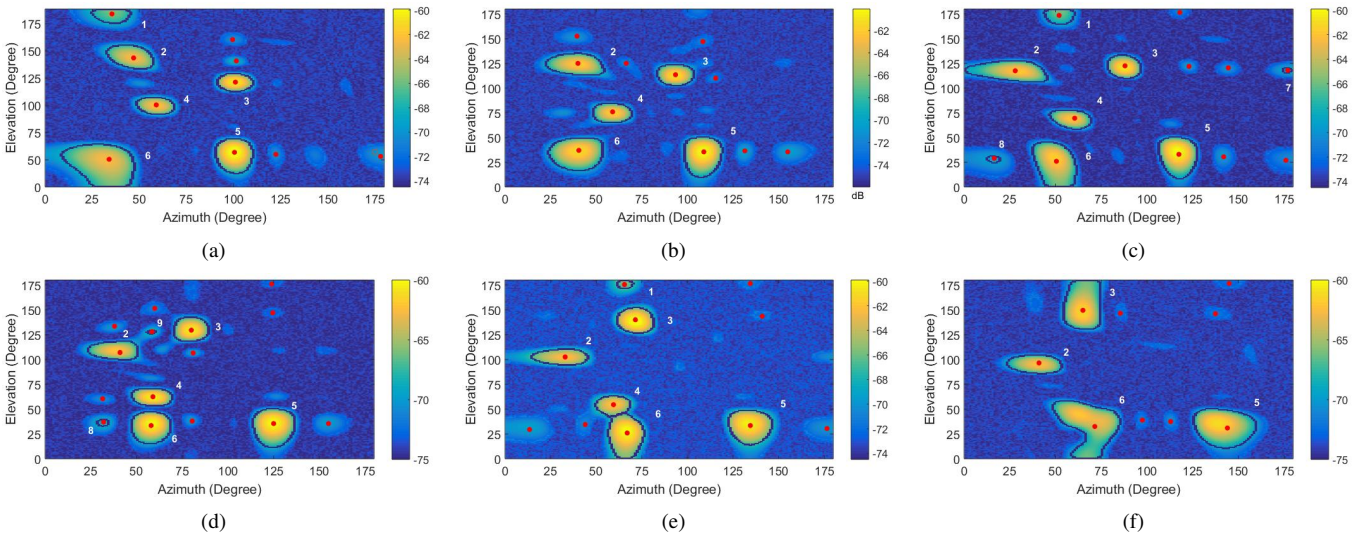

Fig. 12. Cluster recognition and tracking results obtained by using the proposed PASCT algorithm, where (a)-(f) are six consecutive snapshots based on the simulation data.

10(d), where the total cost weight of true moving paths can be obtained by the sum of the selected node-values, as follows:

$$C^* = \sum_{a_i \subset A} v_{a_i} + \sum_{b_j \subset B} v_{b_j} \tag{26}$$

or the sum of the cost weight of the selected nodes, as follows:

$$C^* = \sum_{a_x, b_j \in \mathbf{v}^*} C_{a_x, b_j}. \tag{27}$$

Note that, the K-M approach can also find the true moving paths where $\mathbf{A}$ and $\mathbf{B}$ contain a different number of nodes. However, the K-M approach can only give the moving paths linking the clusters which have similar characteristics, but cannot estimate the situation that one cluster is dead whereas a new cluster appears at the next snapshot. Hence, a maximum mass center moving distance $\Delta C_{\mathrm{T}}^{\mathrm{A}}$ is used for each moving path to decide the birth-death of cluster, e.g., if a moving path $v(a_x, b_y)$ in $\mathbf{v}^*$ is larger than $\Delta C_{\mathrm{T}}^{\mathrm{A}}$, a_x and b_y are recognized as different clusters then, which means that a_x is dead and b_y is a new cluster appearing in the next snapshot.

In addition, due to the non-stationarity of the time-varying channels, the dynamic clusters may rapidly disappear and appear. In this case, a re-tracking process is used to accurately track the dynamic clusters in time-varying channels. As shown in Fig. 11, the circles and the numbers represent the clusters and the tracking IDs of the clusters, respectively. If there are new clusters in the current snapshot, e.g., c_3 and c_4 in snapshot S_i, the tracking algorithm is conducted again between snapshots S_i and S_{i-2} to track clusters in S_i directly from the clusters in S_{i-2}. According to the tracking result, if the new cluster can be tracked to the old cluster in S_{i-2}, the new cluster inherits the tracking ID from the old cluster, e.g., c_3, otherwise, the new cluster is considered as a newborn cluster, e.g., c_4.

Therefore, to accurately track the dynamic clusters in time-varying channels, the newly obtained cluster in snapshot S_i, e.g., c_3 in Fig. 11, is re-tracked to the clusters in snapshot S_{i-2}, e.g., a_3 in Fig. 11 In this case, the dynamic cluster which disappears and appears can still be still tracked, rather than being considered as a new cluster. The pseudocode of the proposed algorithm is provided in the Appendix.

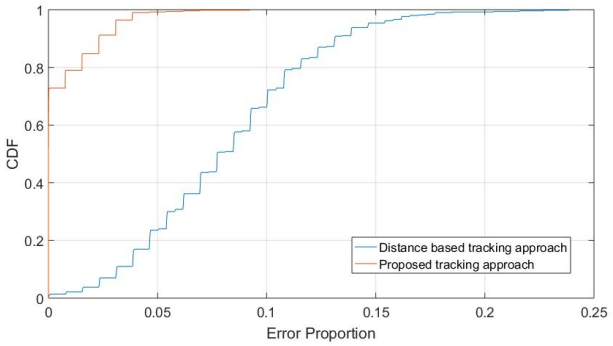

Fig. 13. CDF of error proportion of the proposed tracking approach and the conventional minimum distance based tracking proportion.

V. Validation

This section presents the validation and analysis of the PASCT algorithm based on both simulations and measurements. The measurement-based dynamic channel model in [40] is adopted to generate channels, where different statistical distributions are used to model the azimuth, elevation, and power of cluster-centroids. The performance of the PASCT algorithm can be objectively evaluated by comparing the cluster recognition and tracking results with the ground truth in the simulated channels. Then, the proposed algorithm is tested based on the measurement results to observe the practical performance. In addition, the computational complexity of the PASCT algorithm is also analyzed.

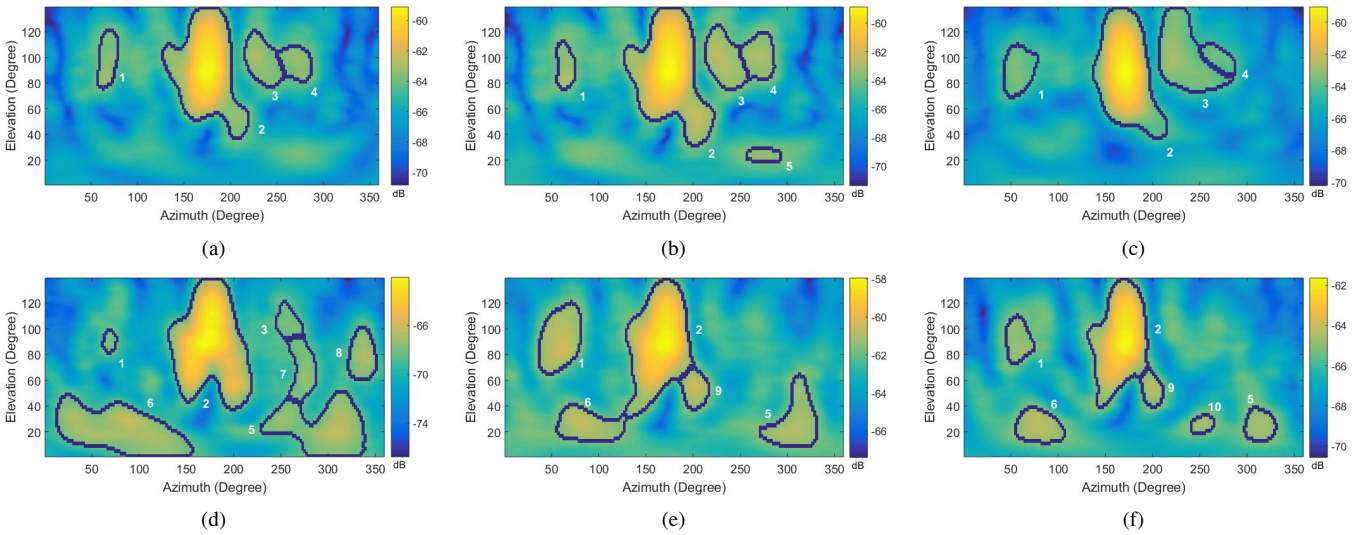

Fig. 14. Cluster recognition and tracking results obtained by using the PASCT algorithm, where (a)-(f) are six consecutive snapshots based on the measurement data in the LoS scenario.

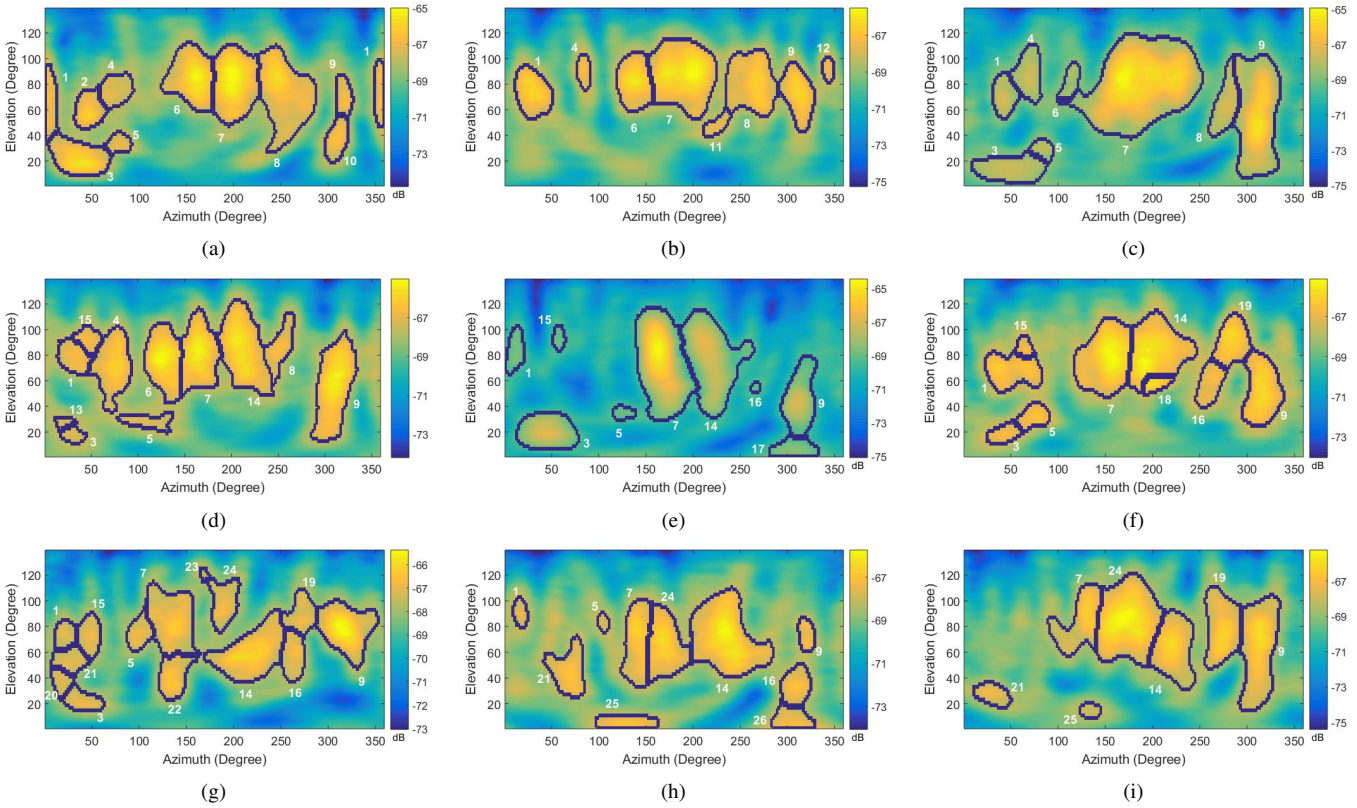

Fig. 15. Cluster recognition and tracking results obtained by using the PASCT algorithm, where (a)-(i) are nine consecutive snapshots based on the measurement data in the NLoS scenario.

A. Validations Based On Simulations

Generally, MPC's parameters have variations within its lifetime, and the variation of dynamic MPCs is widely modeled by using the linear polynomial functions [40]–[43], which have a good tradeoff between the complexity of the proposed channel models and the measurement results. Specifically, as suggested in [40], the cluster's lifetime is modeled by Truncated Gaussian distribution, the number of new clusters are modeled by Gamma distribution, the initial angle distribution and initial power of newborn clusters are modeled by zero-mean Gaussian distribution and a dual-slope model, respectively, and dynamic change of clusters is modeled by linear polynomial functions with different lifetimes. The specific model parameters can be found in the Urban Model in [40]. Then, the MPCs are generated around the cluster-centroids, where the intra-cluster variation is generated based on the channel model proposed in [41]. Then, the Bartlett beamformer [26]

TABLE II
SIMULATION RESULTS

Recognition rate of main clusters	100%
Recognition rate of fragmental clusters	68%
Average angular spread of each cluster	20.15 degrees
Average RMSE of the angular spread of each cluster	3.54 degrees

TABLE III
SIMULATION PARAMETERS AND ALGORITHM PARAMETERS

Parameter	Value	Parameter	Value
Number of clusters	5-10	r	3
Number of snapshots	20	ρ_1	1
$\Delta A_{\max}$	20 (dB)	ρ_2	5
$S_{\max}^{\mathrm{T}}$	2000 (elements)	ρ_3	1
$S_{\min}^{\mathrm{T}}$	20 (elements)	$\Delta C_{\mathrm{T}}^{\mathrm{A}}$	30 (degree)

is used to obtain the PAS based on the generated clusters. A directional 12×12 planar array is adopted, since the antenna radiation pattern does not directly affect the cluster recognition process of the proposed PASCT algorithm. The parameters of the simulation and the PASCT algorithm are summarized in Table III. It is noteworthy that $S_{\min}^{\mathrm{T}}$, $S_{\max}^{\mathrm{T}}$ and $\Delta A_{\max}$ may need to be adjusted for different measured data.

Figs. 12(a)-(f) present an example of using the PASCT algorithm during six consecutive snapshots based on the simulation results, where the recognized clusters are stroked by black outlines, and marked by sequential cluster IDs to clearly present the evolutions. The true cluster-centroids positions are plotted by using red dots in each snapshot. Moving clusters inherit the cluster IDs from the previous snapshots, e.g., clusters 2, 3, 4, 5 and 6 in Figs. 12(a)-(c), whereas new clusters are allocated with new cluster IDs, e.g., clusters 7, 8 and 9 in Fig. 12(c). To further validate the tracking performance, the conventional distance based tracking approach is conducted and compared with the proposed tracking approach through 250 times simulations. Fig. 13 presents the cumulative distribution function (CDF) of the error proportion for both two tracking approaches, which is computed as

$$R^{\mathrm{error}} = \frac{N^{\mathrm{error}}}{N^{\mathrm{path}}} \tag{28}$$

where N^{error} and N^{path} are the numbers of wrong moving paths and whole moving paths, respectively. The proposed tracking approach is designed to find the globe best matching sets of moving paths instead of the minimum distance of moving paths, thus the accuracy of the proposed tracking approach outperforms the conventional minimum distance based tracking approach, as shown in Fig. 13.

To accurately validate the performance of clustering, the clusters are divided into two different types: the clusters with stronger power are defined as the main clusters, e.g., the clusters 2, 3, 4, 5 and 6 in Fig. 12(c), whereas the clusters with weaker power are defined as the fragmental clusters, e.g., the clusters 7, 8 and 9 in Fig. 12(c). The clustering performance of the PASCT algorithm is validated through 250 times simulation, showing 100% recognition rate of the main clusters, whereas 68% recognition rate of the fragmental clusters as summarized in Table II. This is because the strong power of the main clusters makes them easy to be recognized, whereas the fragmental clusters with low power are more difficult to be separated from the background noise. Moreover, the angular spread of each recognized cluster is also calculated and compared with the ground-truth. To validate the accuracy of clustering, the average root-mean-square error (RMSE) of the angular spread of the ground truth and the recognized clusters is given in Table II. It is found that the RMSE of the angular spread is lower than 3.54 degrees, whereas the average angular spread of each cluster is 20.15 degrees. This indicates a good accuracy of the clustering performance. From the simulation results, the PASCT algorithm can well recognize and track the clusters in time-varying channels.

B. Validations Based On Measurements

To properly validate the performance of the PASCT algorithm, the measurement data is divided into i) the LoS scenario and ii) the NLoS scenario, as mention in Section II-B. The parameters of the PASCT algorithm are also set as same as in Table III.

Fig. 14 and Fig. 15 give the cluster recognition and tracking results obtained by using the PASCT algorithm in consecutive snapshots, which are extracted from the measurement data in the LoS and NLoS environments, respectively. As shown in Fig. 14, the main cluster, which has the strongest power and is identified as cluster 2, can be well recognized and tracked during the whole time. Besides, it is found that the fragmental clusters, such as clusters 3, 4 and 7, always appear with small power and keep changing during few snapshots, then disappear at last. This indicates that these fragmental clusters could be the signal reflected from moving objects, such as pedestrians or passing cars. Specifically, it is further found that cluster 1 also exists during the whole time but with lower power compared with the main cluster (cluster 2), which could be caused by distant co-directional cars or dual-reflection signals. On the other hand, there is no particularly main cluster in the NLoS environment, as shown in Fig. 15, where most of the clusters have similar power. Moreover, the number of visible clusters in the NLoS environments is obviously more than in the LoS environments, and the dynamic change of the clusters in the NLoS environments is also more apparent. Specifically, some clusters may disappear and appear in a short time, e.g., cluster 5 in Fig. 14 and clusters 3 and 5 in Fig. 15. Due to the re-tracked process, these dynamic clusters can still be well tracked by the PASCT algorithm.

Moreover, the PASCT algorithm is used to observe the dynamic changes of the clusters during the transition period where the channel changes from LoS to NLoS. Fig. 16 gives cluster recognition and tracking results by using the proposed algorithm, where (a)-(f) are six consecutive snapshots based on the measurement data during the transition from LoS to NLoS environments. It is found that the clusters generally sparsely distribute in angle domain with a higher power in the LoS environment, whereas both the number and size of the

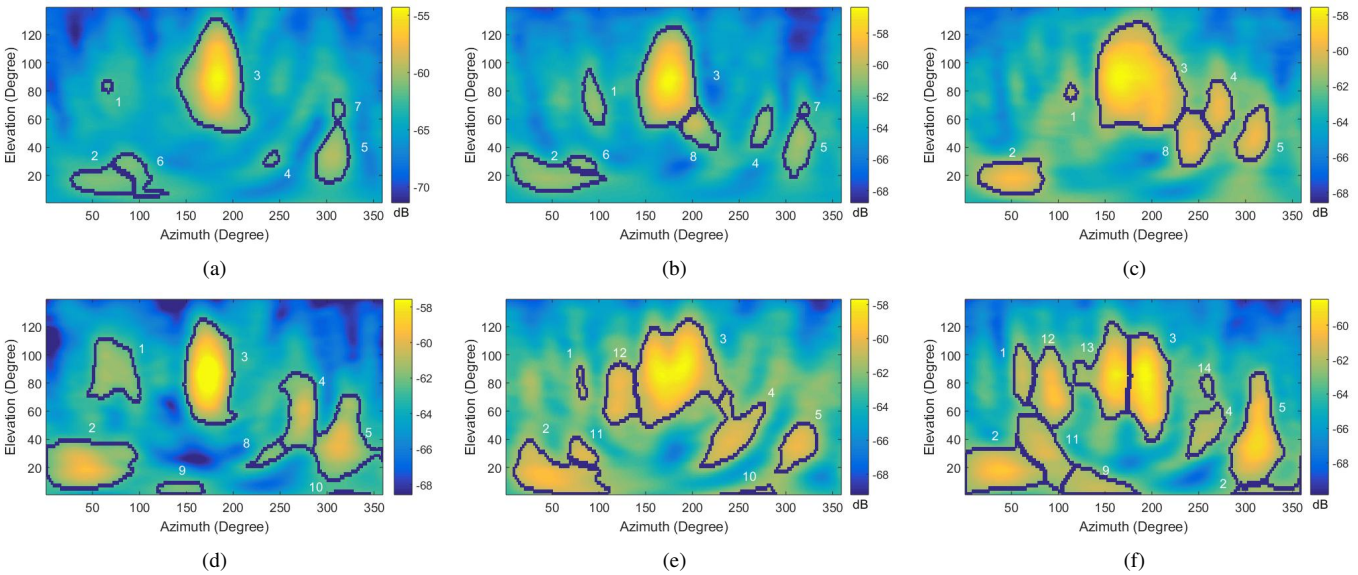

Fig. 16. Cluster recognition and tracking results obtained by using the proposed algorithm, where (a)-(f) are six consecutive snapshots based on the measurement data during the transition of channels from LoS to NLoS environments.

TABLE IV
AVERAGE NUMBER AND LIFETIME OF OBSERVED CLUSTERS

	Average number (In one snapshot)	Average lifetime (second)
LoS Scenario	4.2	11.42
NLoS Scenario	7.3	8.56

clusters are increased in the NLoS scenario, and the power of the clusters is generally decreased. The observation of the transition period conforms to the practical difference between the LoS and NLoS channels.

Furthermore, based on our experiments, statistics of the recognized clusters in the LoS and NLoS scenario are summarized in Table IV. It is found that the clusters in the LoS environment tend to have a longer lifetime. On the other hand, there are usually more clusters appeared but with a shorter lifetime in the NLoS environment.

C. Computational Complexity Analysis

Considering the PASCT algorithm is developed as a low complexity algorithm and provide referential information to channel modeling or other off-line algorithms, the computational complexity is validated and analyzed by counting the average running time of using the PASCT algorithm for each snapshot. The hardware operation platform is the desktop computer with Intel-Core i5-6400 and 8GB random access memory, and the software platform is Matlab R2016a.

To evaluate the computational complexity, the clustering result and running time are compared with the conventional solution with SAGE [21] and KPowerMeans [16], where MPCs are firstly extracted by using SAGE and then clustered with KPowerMeans. In comparison, the number of MPCs is set to be 150 for SAGE implementation, which is found to lead to reasonable results. Then, the cluster identification results and running time of the two solutions are compared.

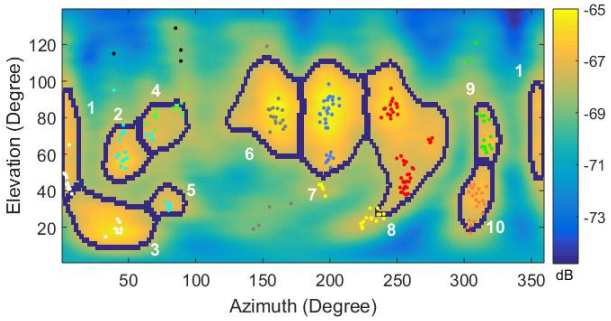

Fig. 17. Comparison of clustering results by using BF+PASCT approach and SAGE+KPowerMeans approach, where the colored dots are MPCs estimated by using SAGE, and the clustering result of KPowerMeans is plotted by different colors.

Fig. 17 shows an example plot of clustering results, where the same measurement data in Fig. 7 are used here. The extracted MPCs are plotted together with the PAS and the different colors of MPCs represent different clusters in Fig. 17. It is found that the most clusters identified by the proposed solution and conventional solution are generally similar, which shows that the proposed solution has fairly good accuracy. Moreover, the running time of conducting the two solutions on 100 snapshots are counted, where the average running times (for each snapshot) of both the two solutions are summarized in Table V, where the BF and PASCT solution can provide results with lower computational cost than the conventional SAGE and KPowerMeans approach. Therefore, based on the experiments, the proposed algorithm is able to achieve fairly good accuracy on the dynamic cluster identification with lower complexity compared to the conventional solution.

VI. CONCLUSION

In this paper, a power angle spectrum based clustering and tracking algorithm is proposed to recognize and track the clus-

TABLE V
AVERAGE RUNNING TIME FOR EACH SNAPSHOT

	running time
BF+PASCT	0.57 s + 0.40 s
SAGE+KPowerMeans	213.33 s + 0.45 s

ters in time-varying channels. Instead of clustering the MPCs extracted by using a high-resolution estimation algorithm, the proposed algorithm directly recognizes and tracks the clusters based on the PASs. Furthermore, to track the recognized clusters, the clusters are characterized in size, position, and shape, where OH is innovatively developed to describe the shape feature of the clusters. The proposed PASCT algorithm is well validated based on both simulations and measurements. Through the experiments, the BF and PASCT solution is able to achieve fairly good accuracy with lower complexity compared to the conventional solution. Besides, the clusters in time-varying channels can be clearly observed by using our algorithm, which can provide statistical information for channel modeling and further studies.

APPENDIX

The pseudocode of the proposed algorithm is presented as follows:

Algorithm 1 A power-angle-spectrum based MPC clustering and tracking algorithm

Input: Obtained PASs: $\mathbf{S} = \{\mathbf{S}_1, \mathbf{S}_2, \cdots, \mathbf{S}_T\}$**,** $\Delta A_{\max}$**,** $\Delta C_{\mathrm{T}}^{\mathrm{A}}$**,** $S_{\min}^{\mathrm{T}}$**,** $S_{\max}^{\mathrm{T}}$**,** $\rho 1$**,** $\rho 2$ **and** $\rho 3$**.**
% Target recognition
for $t = 1 : T$ **do**
  while $S_{\min}^{\mathrm{T}} < S_{\min} \& S_{\max} < S_{\max}^{\mathrm{T}} \& \Delta A < \Delta A_{\max}$ **do**
    $\Delta \alpha'_W = \Delta \alpha'_W + 0.1\alpha'_L$
    Calculate ${\alpha'_T}^*$ using (13)
    Update S and ΔA from the recognized target objects by using ${\alpha'_T}^*$
  end while
  Obtain the target: $\mathbf{X} = \{x_1, x_2, \cdots, x_M | \alpha_{x_i} > {\alpha'_T}^*\}$
  %Cluster separation
  for $m = 1 : M$ **do**
    Calculate ${\alpha'_D}^*$ using (14)
    Clustering the elements in x_i based on ${\alpha'_D}^*$
    Attache the unclustered elements in x_i to the closest element with highest power
  end for
end for
%Tracking process
for $t = 1 : T$ **do**
  Obtained cluster:=$\{a_1^t, a_2^t, \cdots, a_n^t\}$
  Calculate C_a^N, $\mathbf{C}_a^A$ and $\mathbf{C}_a^{OH}$ using (16) and (17)
  Calculate $C_{a_i^t, a_j^t - 1}$ using (18)
  Track clusters based on C^* calculated by using (26)
  if New cluster a_n^t obtained **then**
    Calculate $C_{a_n^t, a_j^t - 2} using (18)$
    Track new cluster based on C^* calculated by using (26)
  end if
end for
Output: Tracked clusters in $\mathbf{S} = \{\mathbf{S}_1, \mathbf{S}_2, \cdots, \mathbf{S}_T\}$**.**

REFERENCES

[1] R. He, O. Renaudin, V.-M. Kolmonen, K. Haneda, Z. Zhong, B. Ai, and C. Oestges, "Characterization of quasi-stationarity regions for vehicle-to-vehicle radio channels," *IEEE Trans. Antennas Propag.*, vol. 63, no. 5, pp. 2237–2251, May 2015.

[2] A. F. Molisch and F. Tufvesson, "Propagation channel models for next-generation wireless communications systems," *IEICE Transactions on Communications*, vol. 97, no. 10, pp. 2022–2034, 2014.

[3] A. A. M. Saleh and R. Valenzuela, "A statistical model for indoor multipath propagation," *IEEE J. Sel. Areas Commun.*, vol. 5, no. 2, pp. 128–137, February 1987.

[4] L. Liu et al., "The COST 2100 MIMO channel model," *IEEE Wireless Commun.*, vol. 19, no. 6, pp. 92–99, Dec. 2012.

[5] 3GPP TSG RAN, "Spatial channel model for multiple input multiple output (MIMO) simulations," 3GPP, Tech. Rep., pp. 1–41, 2004.

[6] J. Meinila, P. Kyosti, T. Jamsa, and L. Hentila, "WINNER II channel models," *Radio Technologies and Concepts for IMT-Advanced*, pp. 39–92, 2009.

[7] R. He et al., "An automatic clustering algorithm for multipath components based on Kernel-power-density," in *Proc. IEEE WCNC, 2017*, San Francisco, USA, March 19-22, 2017, pp. 1–6.

[8] W. Fan, P. Kyosti, J. O. Nielsen and G. F. Pedersen, "Wideband MIMO channel capacity analysis in multiprobe anechoic chamber setups," *IEEE Trans. Veh. Technol.*, vol. 65, no. 5, pp. 2861–2871, 2016.

[9] A. F. Molisch, H. Asplund, R. Heddergott, M. Steinbauer and T. Zwick, "The COST259 directional channel model-part I: Overview and methodology," *IEEE Trans. Wirel. Commun.*, vol. 5, no. 12, pp. 3421–3433, 2006.

[10] J. Karedal, S. Wyne, P. Almers, F. Tufvesson and A. F. Molisch, "A measurement-based statistical model for industrial ultra-wideband channels," *IEEE Trans. Wirel. Commun.*, vol. 6, no. 8, pp. 3028–3037, Aug. 2007.

[11] C. Gentile, "Using the kurtosis measure to identify clusters in wireless channel impulse responses," *IEEE Trans. Antennas Propag.*, vol. 61, no. 6, pp. 3392–3395, June 2013.

[12] R. He et al., "On the clustering of radio channel impulse responses using sparsity-based methods," *IEEE Trans. Antennas Propag.*, vol. 64, no. 6, pp. 2465–2474, June 2016.

[13] R. Xu and D. Wunsch, "Survey of clustering algorithms," *IEEE Transactions on Neural Networks*, vol. 16, no. 3, pp. 645–678, 2005.

[14] R. He et al., "Clustering Enabled Wireless Channel Modeling Using Big Data Algorithms," *IEEE Communications Magazine*, vol. 56, no. 5, pp. 177–183, May 2018.

[15] X. Chen, M. Zhang, S. Zhu and A. Zhang, "Empirical Study of Angular-Temporal Spectra in a Reverberation Chamber," *IEEE Trans. Antennas Propag.*, early access.

[16] N. Czink, P. Cera, J. Salo, E. Bonek, J. P. Nuutinen and J. Ylitalo, "A framework for automatic clustering of parametric MIMO channel data including path powers," in *Proc. IEEE Veh. Technol. Conf. (VTC06)*, 2006, pp. 1–5.

[17] R. He et al., "A Kernel-power-density based algorithm for channel multipath components clustering," *IEEE Trans. Wireless Commun.*, vol. 16, no. 11, pp. 7138-7151, Nov. 2017.

[18] J. Salo, J. Salmi, N. Czink, and P. Vainikainen, "Automatic clustering of nonstationary MIMO channel parameter estimates," in *Proc. Ict05 Cape Town South Africa May Cape Town South Africa*, 2005, pp. 1–5.

[19] P. Hanpinitsak, K. Saito, J. I. Takada, M. Kim and L. Materum, "Multipath clustering and cluster tracking for geometry-based stochastic channel modeling," *IEEE Trans. Antennas Propag.*, vol. 65, no. 11, pp. 6015-6028, Nov. 2017.

[20] Q. Wang et al., "A framework of automatic clustering and tracking for time-variant multipath components," *IEEE Commun. Lett.*, vol. 21, no. 4, pp. 953–956, 2017.

[21] B. H. Fleury, M. Tschudin, R. Heddergott, D. Dahlhaus and K. I. Pedersen, "Channel parameter estimation in mobile radio environments using the SAGE algorithm," *IEEE J. Sel. Areas Commun.*, vol. 17, no. 3, pp. 434–450, Mar 1999.

[22] R. G. Vaughan and N. L. Scott, "Super-resolution of pulsed multipath

channels for delay spread characterization," *IEEE Trans. on Communications*, vol. 47, pp. 343–347, March 1999.

[23] A. Richter, "Estimation of radio channel parameters: models and algorithms," Ph.D. dissertation, Technischen Universitat Ilmenau, Ilmenau, Germany, Dec. 2005.

[24] D. Umansky and M. Patzold, "Design of measurement-based wideband mobile radio channel simulators," in *Proc. 4th IEEE Intemational Symposium on wireless Communication Systems, ISWCS 2007*, Tmndheim, Norway, Oct. 2007, pp. 229–235.

[25] A. Fayziyev and M. Patzold, "An improved iterative nonlinear least square approximation method for the design of measurement-based wideband mobile radio channel simulators," in *Proc. IEEE Advanced Technologies for Communications*, ATC 2011, Danang, Vietnam, Apr. 2011, pp. 106–111.

[26] M. S. Bartlett, "Smoothing Periodograms from Time-Series with Continuous Spectra," Nature, vol. 161, pp. 686–687, 1948.

[27] C. Huang et al., "A novel target recognition based radio channel clustering algorithm" in *Proc. 2018 IEEE International Conference on Wireless Communications and Signal Processing, WCSP 2018*, Hangzhou, China, Oct. 2018, pp. 1–6.

[28] N. Otsu,"A threshold selection method from gray-Level histograms," *IEEE Trans. Syst. Man. Cybern.*, vol. 9, no. 1, pp. 62–66, 1979.

[29] A. Rodriguez, and A. Laio, "Clustering by fast search and find of density peaks," *Science*, vol. 344, no. 6191, pp. 1492–1496, 2014.

[30] N. Dalal and B. Triggs, "Histograms of oriented gradients for human detection," in *Proc. IEEE Computer Society Conference on Computer Vision and Pattern Recognition (CVPR)*, 2005, vol. I, pp. 886–893.

[31] J. Munkres, "Algorithms for the assignment and transportation problems," *J. Soc. Ind. Appl. Math.*, vol. 5, no. 1, pp. 32–38, 1957.

[32] C. Huang, R. He, Z. Zhong, Y. A. Geng, Q. Li and Z. Zhong, "A novel tracking-based multipath component clustering algorithm," *IEEE Antennas Wirel. Propag. Lett.*, vol. 16, pp. 2679–2683, 2017.

[33] O. Renaudin, V. M. Kolmonen, P. Vainikainen and C. Oestges, "Wideband measurement-based modeling of inter-vehicle channels in the 5-GHz band," *IEEE Trans. Veh. Technol.*, vol. 62, no. 8, pp. 3531–3540, 2013.

[34] O. Renaudin, V. M. Kolmonen, P. Vainikainen and C. Oestges, "Car-to-car channel models based on wideband MIMO measurements at 5.3 GHz," in *Proc. EuCAP2009*, pp. 635–639, 2009.

[35] R. He et al., "Vehicle-to-vehicle radio channel characterization in crossroad scenarios," *IEEE Trans. Veh. Technol.*, vol. 65, no. 8, pp. 5850–5861, Aug. 2016.

[36] N. Czink, X. Yin, H. Ozcelik, M. Herdin, E. Bonek, and B. H. Fleury, "Cluster characteristics in a MIMO indoor propagation environment," *IEEE Trans. Wirel. Commun.*, vol. 6, no. 4, pp. 1465C1474, 2007.

[37] V. Agarwal, F. Petrini, D. Pasetto, and D. A. Bader, "Scalable graph exploration on multicore processors," in *Proc. Int. Conf. High Performance Comput., Netw., Storage Anal.*, Nov. 2010, pp. 1–11.

[38] B. H. Fleury, "First- and second-order characterization of direction dispersion and space selectivity in the radio channel," *IEEE Transactions on Information Theory*, vol. 46, no. 6, pp. 2027–2044, Sept. 2000.

[39] H. Wiegand, "An introduction to mathematical ecology.," *Biom. Z.*, vol. 13, no. 3, pp. 219–220, 1971.

[40] R. He et al., "A dynamic wideband directional channel model for vehicle-to-vehicle communications," *IEEE Trans. Ind. Electron.*, vol. 62, no. 12, pp. 7870–7882, 2015.

[41] S. Hur et al., "Proposal on millimeter-wave channel modeling for 5G cellular system," *IEEE J. Sel. Top. Signal Process.*, vol. 10, no. 3, pp. 454–469, Apr. 2016.

[42] L. Bernad et al., "Complexity reduction for vehicular channel estimation using the filter divergence measure," in *Proc. IEEEAsilomarConf. Signals, Syst. Comput.*, 2010, pp. 141–145.

[43] Y. Chen and V. K. Dubey, "Dynamic simulation model of indoor wideband directional channels," *IEEE Trans. Veh. Technol.*, vol. 55, no. 2, pp. 417–430, Mar. 2006.